4 • Earth's orbital parameters and cycle stratigraphy

L. A. HINNOV

The Milankovitch theory that quasi-periodic oscillations in the Sun-Earth position have induced significant 10^4–10^6-year-scale variations in the Earth's stratigraphic record of climate is widely acknowledged. This chapter discusses the Earth's orbital parameters, the nature of orbitally forced incoming solar radiation, fossil orbital signals in Phanerozoic stratigraphy, and the use of these orbital signals in calibrating geologic time.

4.1 INTRODUCTION

Over the past century, paleoclimatological research has led to wide acceptance that quasi-periodic oscillations in the Sun–Earth position have induced significant variations in the Earth's past climate. These orbitally forced variations influenced climate-sensitive sedimentation, and thereby came to be fossilized in the Earth's cyclic stratigraphic record. The detection of orbital variations in Earth's cycle stratigraphy was progressively facilitated by advancements in celestial mechanics, which have provided more accurate models of the Earth's orbital–rotational behavior through geological time, and by improvements in data collection and analysis.

A principal outcome of the research has been the recognition that cycle stratigraphy, when shown to carry the signal specific to Earth's orbital behavior, serves as a powerful geochronometer. High-quality data collected over the past decade, in particular, have proven to have faithfully recorded all of the orbital cycles predicted by modern celestial mechanics over 0–23 Ma. Consequently, for the first time, the entire Neogene Period has been astronomically calibrated, and is reported in Chapter 21 as the Astronomically Tuned Neogene Time Scale 2004 (ATNTS2004). Cycle stratigraphy from more remote geological ages has not yet been calibrated directly to the orbital cycles, because of model limitations and greater uncertainties in determining stratigraphic age. Nonetheless, in numerous instances signal components analogous to those of the orbital variations have been detected in cycle stratigraphy, prompting the development of "floating time scales" that are calibrated to the average value of one or several model orbital frequencies. In Chapters 17–19, orbitally calibrated floating time scales are presented for intervals that extend through entire stages of the Mesozoic periods.

This chapter provides an introduction to the Earth's orbital parameters, the nature of the orbitally forced incoming solar radiation (insolation), and the discovery of orbitally forced insolation signals in cycle stratigraphy. The chapter concludes with remarks on the precision and accuracy that can be expected from orbitally calibrated cycle stratigraphy.

4.2 EARTH'S ORBITAL PARAMETERS

The Earth undergoes quasi-periodic changes in its orientation relative to the Sun as a consequence of interactions between the Earth's axial precession and variable orbit induced by motions of the other planets. These changes are described in terms of the Earth's *orbital parameters* (Fig. 4.1). Quantification of the orbital parameters has been carried out numerous times in the past with analytical approximations of the planetary motions (e.g. Milankovitch, 1941; Bretagnon, 1974; Berger, 1977a,b; Berger *et al.*, 1989; Laskar, 1990). Today, orbital models are performed largely by computerized numerical integration, and while they continue to share many of the features contained in the earlier ones, important new variables have been included, e.g. relativitistic effects, Earth's tidal braking, dynamical ellipticity, climate friction, Sun's oblateness, etc. For example, the model of Laskar *et al.* (1993) is reported as $La93_{(CMAR,FGAM)}$, where CMAR is input for the tidal effect of the Moon and FGAM is the input for the dynamical ellipticity of the Earth. The nominal model $La93_{(0,1)}$ assumes no tidal friction and present-day ellipticity; $La93_{(1,1)}$ builds in the tidal effect of Quinn *et al.* (1991). La93 provides an accurate "ephemeris" for the past 16 million years; uncertainties in the model's initial conditions and indications for chaotic motions of the planets impose an absolute accuracy limit at about 32 myr BP (Laskar, 1999).

A Geologic Time Scale 2004, eds. Felix M. Gradstein, James G. Ogg, and Alan G. Smith. Published by Cambridge University Press.

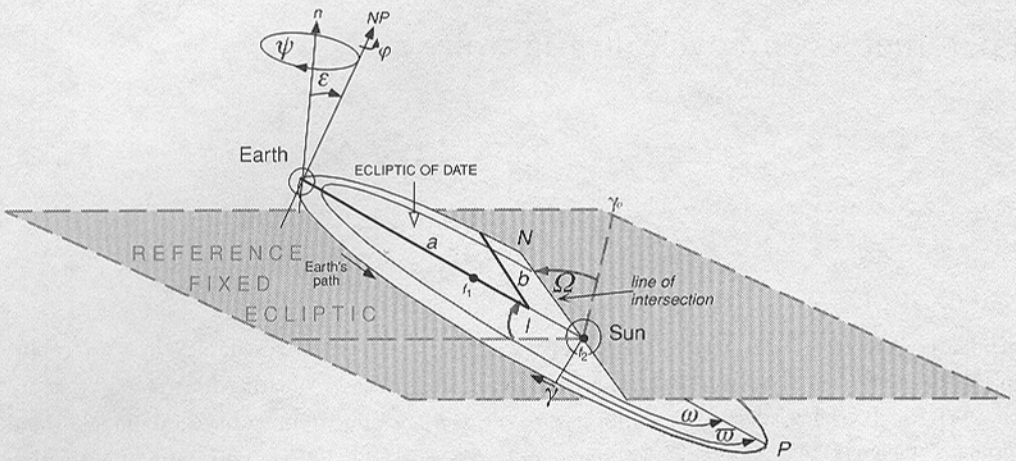

Figure 4.1 The Earth's orbital parameters seen from a view above the Earth's geographic North Pole (NP) in a configuration of northern summer solstice (NP pointed toward the Sun). The Earth's orbit is elliptical with (invariant) semi-major axis a and semi-minor axis b defining eccentricity e. The Sun occupies one of the two foci (f_1, f_2). Variables e, Π, I and Ω are "orbital elements," where $\Pi = \Omega + \omega$. The plane of the Earth's orbit (the "ecliptic of date") is inclined an angle I relative to a fixed reference ecliptic, and intersects this plane at a longitude Ω at point N, the ascending node, relative to fixed vernal point γ_0. (In this depiction, I is greatly exaggerated from its actual magnitude of only 1 to 2°.) The orbital perihelion point P is measured relative to γ_0 as the longitude of perihelion Π, and moves slowly anticlockwise. The Earth's figure is tilted with respect to the ecliptic of date normal n at obliquity angle ε. Earth's rotation φ is anticlockwise; gravitational forces along the ecliptic of date from the Moon and Sun act on the Earth's equatorial bulge and cause a clockwise precession Ψ of the rotation axis. This precession causes the vernal equinox point γ to migrate clockwise along the Earth's orbit, shifting the seasons relative to the orbit's eccentric shape; this motion constitutes the "precession of the equinoxes." The angle ω between γ and P is the moving longitude of perihelion and is used in the precession index $e\sin\omega$ to track Earth–Sun distance. Variations of e, ε, and $e\sin\omega$ are shown in Fig. 4.2.

According to $La93_{(0,1)}$, over the past 10 million years the Earth's *orbital eccentricity* varied from 0 to ~7% (Fig. 4.2*a*) with principal modes at 95, 99, 124, 131, 404, and 2360 kyr (Fig. 4.3*a*), caused by gravitational perturbations from motions of the other planets acting on Earth's orbital elements Π and e (Fig. 4.1). The *obliquity* variation has involved changes in the Earth's axial tilt between 22 and 24° (Fig. 4.2*b*), with a principal mode at 41 kyr, and lesser ones at 39, 54, and 29 kyr (Fig. 4.3*b*), due to planetary motions acting mainly on orbital elements I and Ω (Fig. 4.1). The *precession index* represents the combined effects of orbital eccentricity and the Earth's axial precession on the Sun–Earth distance (Fig. 4.2*c*), and has principal modes at 24, 22, 19, and 17 kyr (Fig. 4.3*c*). Long-period modulations of the obliquity and precession index (Figs. 4.2*b,c*) can be traced to the secular motions of individual planets (e.g. Berger and Loutre, 1990); frequency components of these modulations are summarized in Hinnov (2000).

Over geological time, dissipation of tidal energy is thought to have slowed the Earth's rotation rate (e.g. Berger *et al.*, 1989). This deceleration, accompanied by lunar recession, a declining Earth ellipticity and axial precession rate, would have resulted in a progressive lengthening of the obliquity and precession index modes toward the present (Berger *et al.*, 1992). Table 4.1 presents model predictions for the shortening of the major obliquity and precession index modes over the past 500 Ma, indicating significant changes over the Phanerozoic Eon. In addition, climate friction, i.e. episodic glacial loading of the Earth's crust, may result in "obliquity–oblateness feedback" and possibly significant deviations in the average obliquity angle (e.g. Bills, 1994; Rubincam, 1995). In contrast, orbital eccentricity is independent of geodynamical effects, and, although chaotic motions of some of the planets could destabilize some of the eccentricity modes from their current values, others, in particular the 404 kyr mode, may have remained relatively stable over much of Phanerozoic time (Laskar, 1999).

A newly updated orbital model, $La2003_{(CMAR,FGAM,CLIM)}$ exploits recent advances in numerical integration techniques and promises high-precision computations of the orbital parameters over geological times up to 40 Ma. This new model also provides a third parameter, CLIM, to include the aforementioned climate friction effect (CLIM = 0 assumes no effect). Differences between La93 and La2003 are noticeable at times previous to 20 Ma, and are discussed further in Chapter 21, where the ATNTS-2004 is calibrated to $La2003_{(1,1,0)}$ back to the Oligocene–Miocene boundary (23.03 Ma).

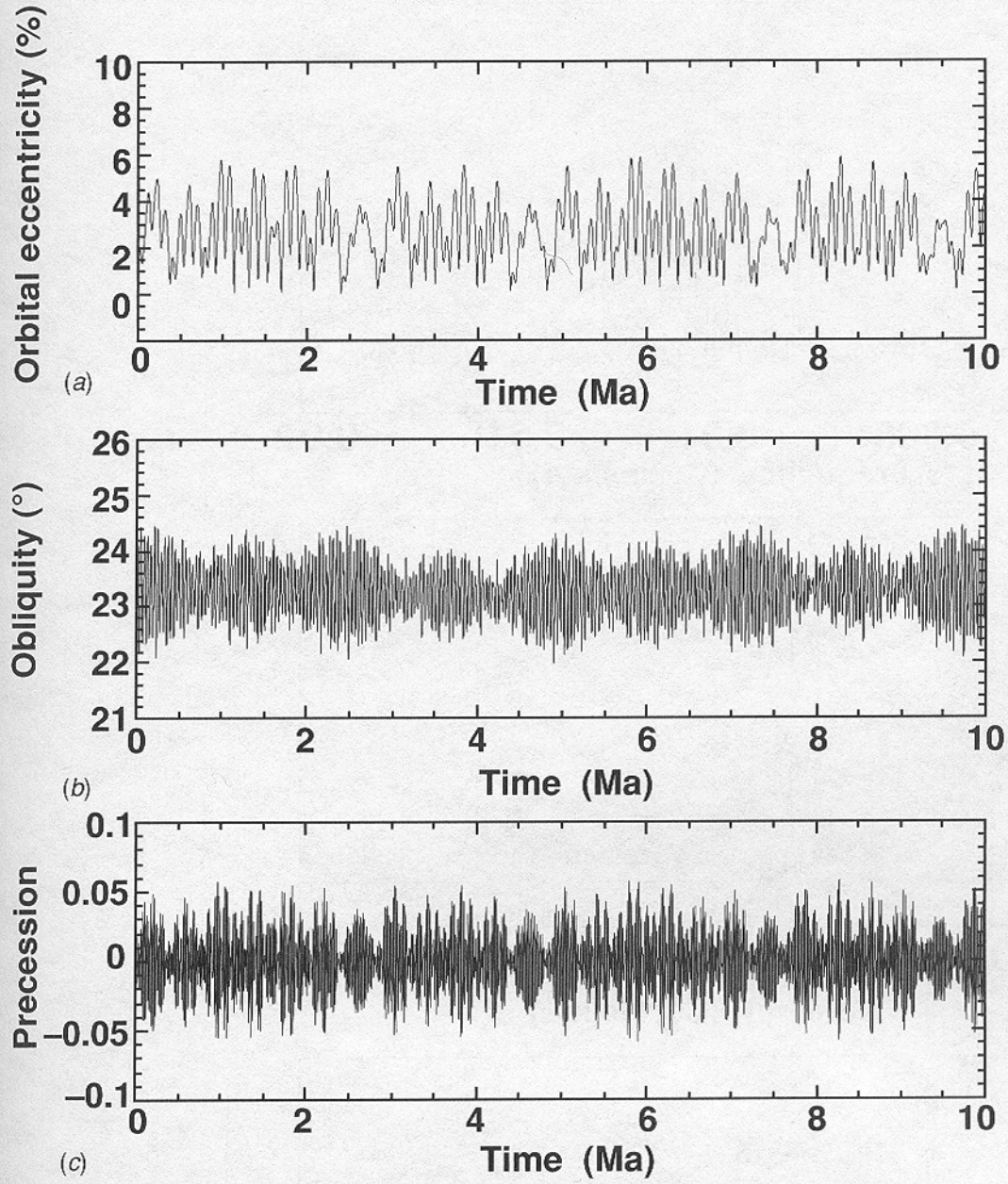

Figure 4.2 Variation of the Earth's orbital parameters over the past 10 million years according to $La93_{(0,1)}$, assuming Earth's present-day ellipticity and rotation rate. (*a*) Orbital eccentricity, in percent; (*b*) obliquity variation, in degrees of axial tilt; (*c*) precession index, in standardized units (dimensionless). All values are from *Analyseries* (Paillard *et al.*, 1996), which calculates $La90(=La93_{(0,1)})$. A FORTRAN code to calculate adjustable models $La93_{(CMAR,\ FGAM)}$ can be downloaded from http://xml.gsfc.nasa.gov/archive/catalogs/616063/index_long.html.

4.3 ORBITALLY FORCED INSOLATION

The orbital parameters affect changes in the intensity and timing of the incoming solar radiation, or insolation, at all points on the Earth. These insolation changes comprise the well-known "Milankovitch cycles" (Milankovitch, 1941; re-issued in English in 1998). Geographical location, time of year, and even the time of day all determine the relative contributions of the orbital parameters to the inter-annual insolation (e.g. Berger *et al.*, 1993). For example, the insolation curves in Fig. 4.4 depict the globally available spectral power of orbitally forced daily insolation at the top of the atmosphere on June 21 (solstice) and March 21 (equinox). These curves are idealized in the sense that it is unlikely that climate responds to insolation only on one day of the year, but integrates insolation over certain times of the year and collectively over specific geographic

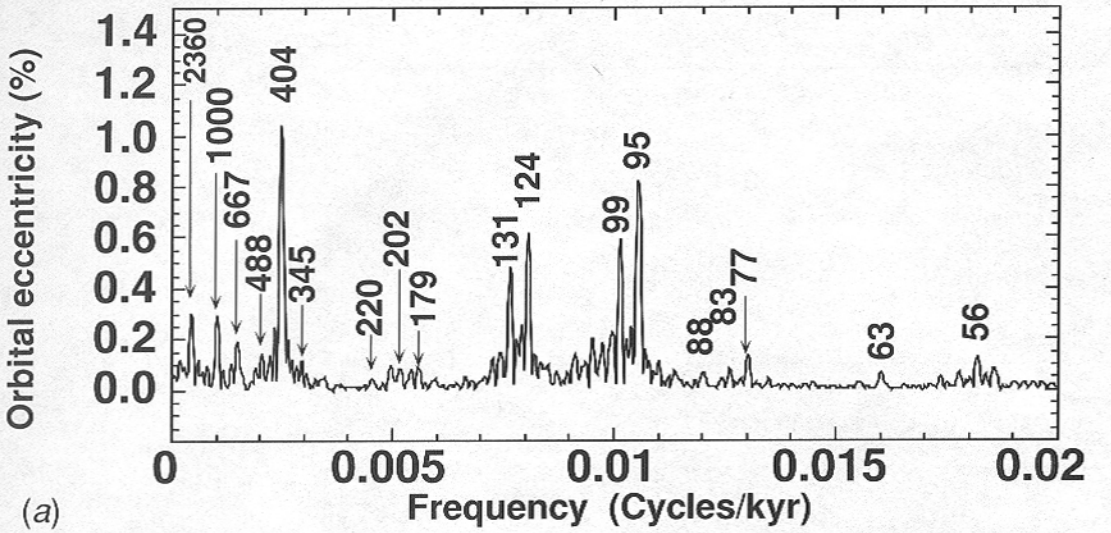

(*a*)

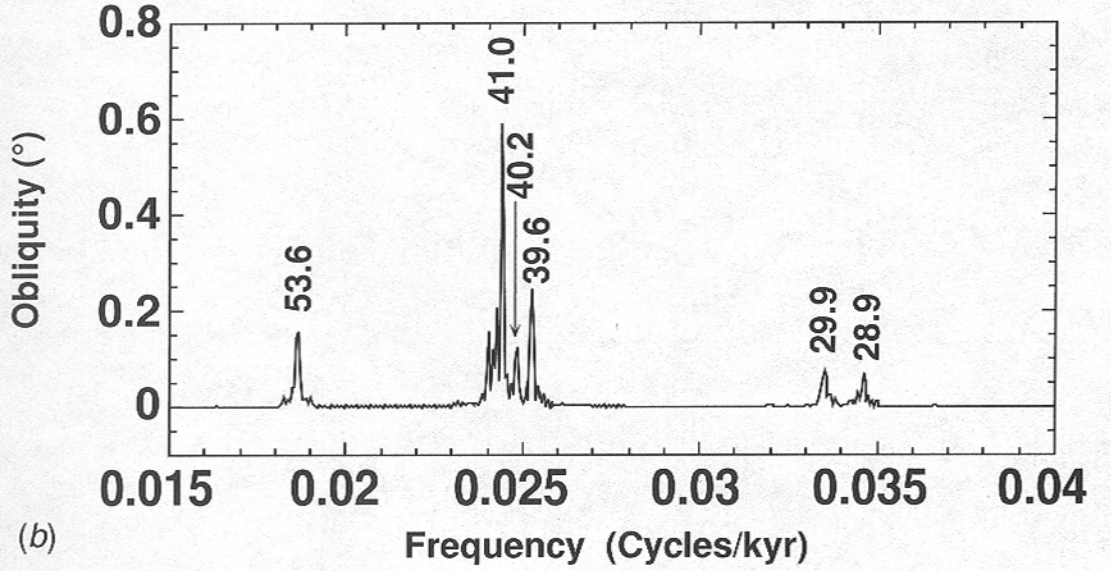

(*b*)

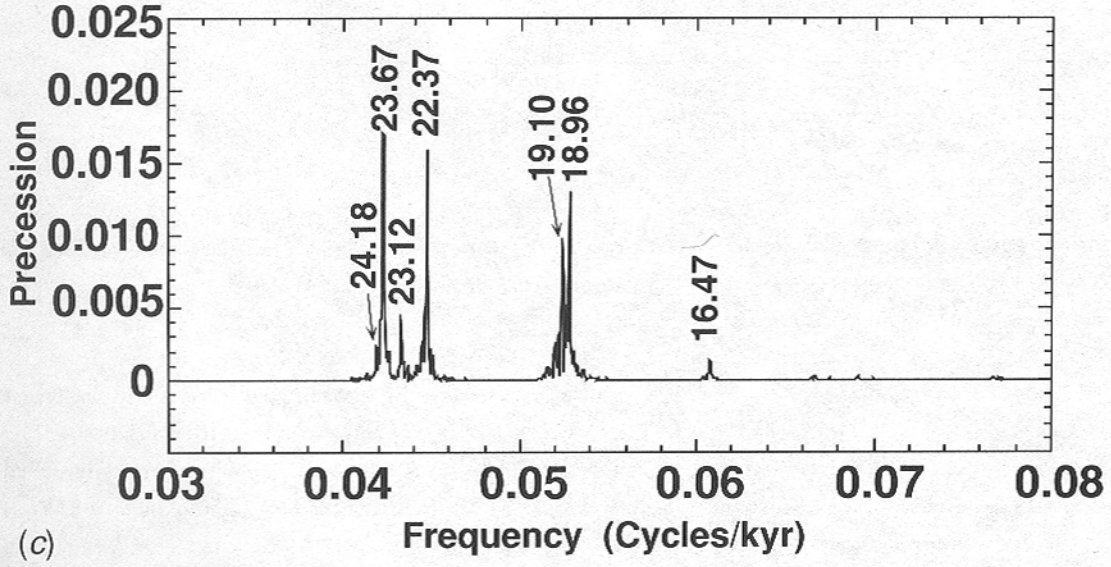

(*c*)

Figure 4.3 Harmonic analysis of the Earth's orbital parameters depicted in Fig. 4.2. All labels identify periodic components in thousands of years that pass the F-ratio test of Thomson (1982) for significant lines above the 95% level, using 4π multi-tapers. (*a*) Orbital eccentricity, (*b*) obliquity variation, (*c*) precession index. (Note: Due to the quasi-periodic nature of the parameters, the significance, periodicity, and amplitude of the labeled signal components will change for analyses over different time segments.)

Table 4.1 *Model of changes in the main periods of the Earth's obliquity variation and precession index*[a]

Time (Ma)	41-kyr mode	39-kyr mode	54-kyr mode	29-kyr mode
OBLIQUITY VARIATION				
0	41 057	39 663	53 805	28 929
72	39 333	38 052	50 883	28 062
270	34 820	33 812	43 577	25 687
298	34 203	33 231	42 615	25 350
380	32 426	31 550	39 891	24 360
440	31 168	30 358	38 003	23 643
500	29 916	29 169	36 158	22 916

Time (Ma)	24-kyr mode	22-kyr mode	19-kyr mode	16.5-kyr mode
PRECESSION INDEX				
0	23 708	22 394	18 966	16 470
72	23 123	21 871	18 590	16 188
270	21 485	20 401	17 517	15 368
298	21 249	20 188	17 359	15 247
380	20 549	19 555	16 889	14 884
440	20 037	19 090	16 542	14 612
500	19 512	18 613	16 182	14 332

[a] As in Hinnov (2000), based on Berger and Loutre (1994, their Table 2, Model 2). Values are in thousands of years.
(Note: The precessional 16.5-kyr mode was calculated using $g = 1/(45\,865$ yr), from Laskar (1990).)

areas, possibly different areas at different times. This "climatic filtering" serves to alter the relative contributions of the orbital parameters to the total output climate response, this even prior to internal climate system responses to the insolation. Thus, it is left to the discretion of the paleoclimatologist to determine which time(s) of the year and at which location(s) a prevailing climate responded to insolation; this can require considerable insight into the infinite number of ways that one can sample insolation in space–time (Rubincam, 1994).

4.4 ORBITAL SIGNALS IN CYCLE STRATIGRAPHY

The prospect that orbital variations exerted large-scale climatic changes that could be detected in the geologic record was already being debated in the nineteenth century (e.g. Herschel, 1830; Adhémar, 1842; Lyell, 1867; Croll, 1875). Gilbert (1895) was the first to attribute the origin of limestone/shale cyclic strata of the Cretaceous Niobrara chalks (Colorado, USA) to astronomical forcing. Bradley (1929) counted varves in the lacustrine oil-shale–marl cycles of the Eocene Green River Formation (Utah, USA) estimating an average 21 630-year time scale for the cycles, and pointing to the precession of the equinoxes as a potential cause. Milankovitch (1941) was the first to attempt a quantitative correlation between astronomically calculated insolation minima and Late Quaternary Ice Age deposits of the Alps. However, later radiocarbon studies of glaciation timings in North America did not clearly corroborate Milankovitch's insolation calculations, and the orbital theory fell into disfavor (see the review in Imbrie and Imbrie, 1979; see also the update in Broecker and Denton, 1989).

At the same time, significant progress was made in understanding the origins of the prevalent rhythmic stratification of Mesozoic Alpine limestones (e.g. Schwarzacher, 1947, 1954). This research culminated in the seminal work of Fischer (1964), who found that the meter-scale beds (the Lofer cyclothems) of the Triassic Dachstein Limestone contained vertically repeating facies indicative of shallow marine environments exposed to oscillating sea levels, with an ~40 kyr timing. However, glaciations were unknown for the Triassic, raising doubts about the mechanisms by which such sea-level oscillations could have occurred; the origin of the Lofer cyclothems continues to be debated today (e.g. Schwarzacher, 1993; Enos and Samankassou, 1998).

It was not until investigation of the Late Quaternary deep-sea sedimentary record was undertaken that Milankovitch's theory of climate change was firmly validated. Emiliani (1955, 1966) explained oxygen isotope fractionation in marine calcareous microfauna as a function of ocean temperature and salinity; subsequently, Dansgaard and Tauber (1969) demonstrated that

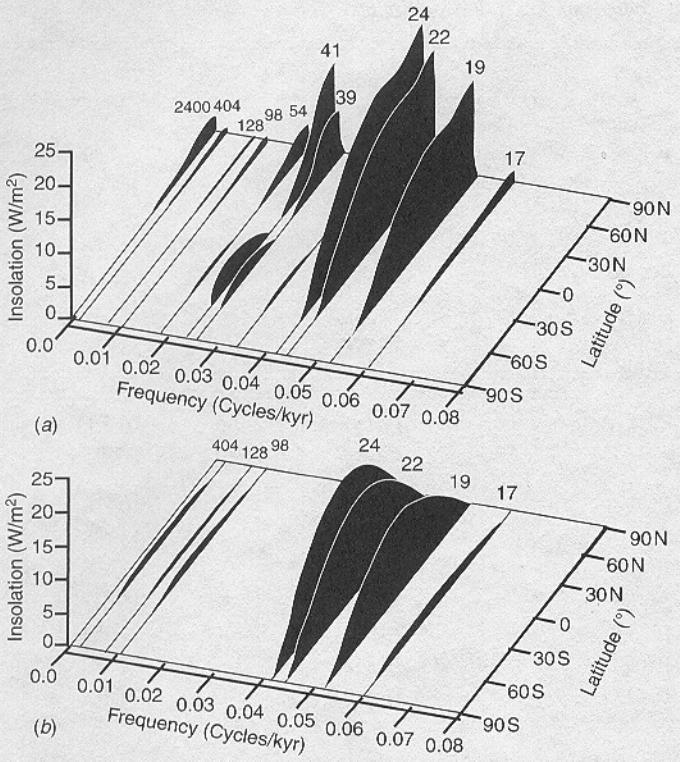

Figure 4.4 Frequency distribution of inter-annual insolation (Laskar, 1990) over 0–5 million years ago, sampled at 1-kyr intervals and displayed as amplitude spectra with respect to geographic latitude. (*a*) Daily mean insolation on June 21 (solstice). Latitudes south of ~66° S receive no insolation on this day. Maximum daily insolation occurs in the northern polar region, which experiences 24-hour exposure. The phase of the eccentricity and obliquity remains constant at all latitudes; for the precession phase shifts progressively from 0 to 180° from month to month (not depicted). (*b*) Daily mean insolation on March 21 (equinox). Insolation strength is a function of local solar altitude, highest at the Equator on this day of equal-time exposure everywhere. Contributions from the obliquity variation are absent. The phase of the eccentricity is constant at all latitudes; for the precession phase shifts progressively from 0 to 180° from pole to pole (not depicted). (Additional notes: (i) Insolation for the December 21 solstice similar to *a*, but with reversed latitudes; and the September 21 equinox is practically identical to *b*. (ii) The precession component of variation in *a* is at all locations 90° out of phase with the precession component in *b*. Additional examples are given in Berger *et al.*, 1993.)

the majority of changes in the marine oxygen isotope fractionation were linked to ocean volume. This result was followed by the landmark study of Hays *et al.* (1976) in which the oxygen isotope record was quantitatively linked to the Milankovitch cycles. Bolstered by the advent of global paleomagnetic stratigraphy, it was subsequently discovered that the same isotope signal, now encompassing the entire Brunhes chron (from 0 to 0.78 Ma), was present in all of the major oceans (Imbrie *et al.*, 1984). Finally, calibration of this proxy for global ocean volume to geological evidence for large sea-level changes (Chappell and Shackleton, 1986) established, albeit indirectly, the connection between the Quaternary Ice Ages and Milankovitch cycles. Later research into polar ice stratigraphy uncovered other isotope signals with strong orbital frequencies, providing additional, overwhelming support for the orbital forcing theory (Petit *et al.*, 1999).

These milestone studies touched off multiple initiatives to search for orbital cycles in stratigraphy back through geologic time using isotopes as well as other climate proxies, including facies stratigraphy, percent carbonate, biogenic silica, magnetic susceptibility, wireline logs, and grayscale scans (see Table 4.2). Continental Plio–Pleistocene sediments recovered from Lake Baikal revealed a strong biogenic silica signal closely mimicking that of the marine isotope record (Williams *et al.*, 1997; Prokopenko *et al.*, 2001). Additional deep-sea drilling yielded a continuous oxygen isotope signal spanning 0–6 Ma (Shackleton, 1995), and today, there is near-continuous Milankovitch coverage back through the Eocene from combinations of various marine climate proxies from both deep-sea drilling and outcrop studies (see Chapters 20 and 21). Evidence for orbital forcing has also been found in Cretaceous pelagic stratigraphy (see Chapter 19) and in Jurassic formations (see Chapter 18). The thick Upper Triassic continental lacustrine deposits of eastern North America contain a nearly perfect eccentricity signal that modulates facies successions linked to wetting–drying climate cycles at precessional time scales (see Chapter 17). It should be noted that cycle stratigraphy much older than ~20 Ma may never successfully be correlated directly to the orbital cycles, but only indirectly though comparison of average signal characteristics between data and orbital theory.

For geologic times prior to the Late Triassic, evidence for orbitally forced stratigraphy is less clear. One reason is that pre-Jurassic oceanic sediments are not composed of the abundant, continuous rain of pelagic oozes as are post-Jurassic ones. Therefore research has focused largely on the more prolific shallow-marine record, for which the primary evidence of Milankovitch forcing is systematic "interruption" rather than a continuous recording (Fischer, 1995). Definitive evidence for orbital signals in the Paleozoic is still weaker. The Permian Castile Formation, a marine evaporite sequence, shows a strong, but apparently short-lived Milankovitch signal (Anderson, 1982). The spectacular shelf carbonate cycles

Table 4.2 *Commonly measured sedimentary parameters that have been linked to orbitally forced climate change, and inferred climate conditions*

	Sedimentary parameter	Associated climate conditions
EXTRINSIC[a] (independent of sedimentation rate)	Oxygen isotopes	Temperature/salinity/precipitation/eustasy
	Carbon isotopes	Productivity/C-sequestration/redox conditions Surface hydrology
	Clay assemblages	
	Microfossil assemblages	Salinity/temperature
INTRINSIC[b] (directly related to and/or influenced by sedimentation rate)	Percent $CaCO_3$, Si, C_{org}	Productivity
	Magnetic susceptibility	Sedimentation rate
	Microfossil abundance	Productivity
	Clay/dust abundance	Surface hydrology/atmospheric circulation
	Lithofacies	Depositional environment
	Sediment color	Productivity/redox conditions
	Grain size	Erosion intensity/hydrodynamics

[a] Extrinsic parameters vary independently from sediment supply.
[b] Intrinsic parameters are directly related to sediment supply, and their signals tend to be more dramatically influenced (distorted) by changes in sedimentation rate (Herbert, 1994).

of the Pennsylvanian Paradox Basin (Utah, USA) indicate high-frequency sea-level oscillations with some orbital signal characteristics (Goldhammer *et al.*, 1994). The classic transgressive–regressive cyclothems of mid-continental USA (e.g. Heckel, 1986) and the rhythmic Mississippian hemipelagic limestones of Ireland (Schwarzacher, 1993) appear to express the dominant 404-kyr eccentricity cycle. There are at present only a few reports of orbital-scale cycles in Devonian formations (e.g. Elrick, 1995; Yang *et al.*, 1995; Bai, 1995; Crick *et al.*, 2001) and fewer still for the Silurian (Crick *et al.*, 2001; Nestor *et al.*, 2001). The thick Cambrian–Ordovician cyclic carbonate banks found world-wide, on the other hand, show some evidence of Milankovitch forcing (Bond *et al.*, 1991; Bazykin and Hinnov, 2002); however, the origins of the vast majority of these high-frequency eustatic signal proxies remain uninvestigated (e.g. Osleger, 1995).

4.5 ESTIMATING ORBITAL CHRONOLOGIES

Early on, the time predictability of the Earth's orbital parameters led to the practice of using orbitally forced cycle stratigraphy as a high-resolution geochronometer. While this application had already been considered by Gilbert (1895) and Barrell (1917), it was Milankovitch (1941) who first calibrated theoretical orbital insolation directly to the geologic record, adjusting approximately known ages of the Late Quaternary Alpine Ice Ages to the insolation minima of his calculated curves. The most significant advances in orbital chronology took place during the latter half of the twentieth century with the development of a high-resolution global marine oxygen isotope stratigraphy and magnetostratigraphy for the Pleistocene Epoch (see the review in Kent, 1999).

True orbital time calibration is possible only for cycle stratigraphy that can be connected to the "canonical" orbital variations, i.e. those quantitatively predicted by orbital theory. In GTS2004, this involves cycle stratigraphy back to the Miocene–Oligocene boundary only (0–23.03 Ma). Calibration of a sequence of cyclic strata begins with the assumption of a target orbital curve. This may take the form of an orbitally forced insolation signal, which most likely affected climate and was subsequently recorded by sedimentation (e.g. the 65° N summer insolation), or it can be as simple as the sum of the standardized orbital parameters (e.g. the ETP curve of Imbrie *et al.*, 1984). This initial assumption, however, introduces a basic source of error, because the true nature of the orbital forcing of the sediment is not known exactly. To account for this, Hilgen *et al.* (2000a), for example, calibrated ("tuned") their Miocene marl–clay deep-sea cycles to two possible target curves, the 65° N summer insolation and the precession index, correlating the mid points of the marls to the centers of the insolation maxima and precession minima. These two calibrations produced chronologies that differed from cycle to cycle by several thousand years; this was taken as a fair representation of the uncertainty of the chronology. Questions remain about which model produces the most accurate orbital cycles

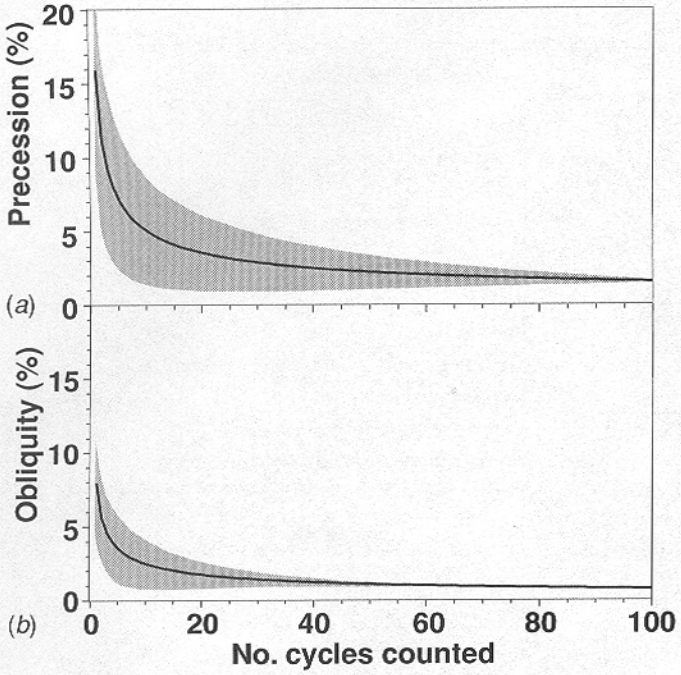

Figure 4.5 Estimated error in measuring time in using orbitally forced cycle stratigraphy when assuming that each cycle represents a duration equal to the average period of the orbital parameter that forced its formation (the "metronome" approach discussed in Herbert *et al.*, 1995). (*a*) Precession index (average period 21 kyr), (*b*) obliquity variation (average period 41 kyr). The curves indicate substantial reductions in potential error for longer time measurements over extended numbers of sequential cycles. The gray envelopes indicate the dispersion (1-sigma level) of this error to account for the high quasi-periodicity of these two orbital parameters (based upon $La93_{(0,1)}$) over short time spans.

back through time, insofar as contributions from Earth's tidal dissipation and dynamical ellipticity have been only partially explored and only in Plio–Pleistocene data (see further discussion in Chapter 21 relating to potential timing errors in ATNTS2004).

Floating orbital time scales (i.e. time scales that are disconnected from canonical orbital variations) are based upon the assumption that frequency components observed in cycle stratigraphy can be related to one or several frequencies predicted by orbital theory. This requires an additional, provisional assumption that planetary motions were stable back to the geological time represented by the data, and that current models of tidal dissipation and dynamical ellipticity which predict progressively shorter orbital periodicities back through time (e.g. Berger *et al.*, 1992) are accurate. This assumption, however, remains largely untested for times prior to the Oligocene, although some studies have shown that numerous key similarities between Earth's data and the current orbital models appear to have existed during geological times as remote as the Triassic (e.g. Olsen and Kent, 1999). Herbert *et al.* (1995) suggested that in some cases it may be possible to "lock on" to individual frequency components of the precession, for example, to obtain high-resolution orbitally calibrated time scales. Such calibrations are typically limited to counting stratigraphic cycles by visual inspection and assume an average orbital cycle period, e.g. 21 kyr for precession, for each cycle. Nevertheless, even this approach, if conducted on perfectly recorded sequences of orbitally forced cycles, can result in highly accurate floating time scales (Fig. 4.5), with uncertainties at only a few percent for only a few tens of cycles counted.